Co-ordinated Grid Forming Control of AC-side-connected Energy Storage Systems for Converter-Interfaced Generation

Junru Chen[1]*, Muyang Liu[1], Renqi Guo[2], Nan Zhao[2], Federico Milano[2], and Terence O'Donnell[2]
Xinjiang University, Urumqi, China
University College Dublin, Dublin, Ireland

Abstract

Grid forming control of converter interfaced generation (CIG) requires some form of energy storage to be coupled with the generation. Energy storage systems (ESSs) can be coupled to the CIG either on the DC or the AC side of the power converter. When placed on the DC side, the ESS can provide damping of the variability in the generation but would require significant modification to the wind turbine hardware. The solution with an ESS connected to the AC side is simpler to implement with existing wind turbines but fails to provide damping of the CIG generation. This paper proposes a grid forming control strategy, based on virtual synchronous generator (VSG) control, which allows the ESS installed at the AC-side of the converter to have the same features and dynamic behaviour as those obtained from placement on the DC-side of the converter. In addition, the proposed control can also limit the exchanged power of the ESS within its rating for a safe operation. The proposed control is validated via a detailed Electro-Magnetic Transient (EMT) model and its impact on the grid is quantified via the case study of the All-Island Irish transmission system. Simulation results show that only a small ESS capacity can ensure that the frequency variance satisfies the grid code requirement even in the situation of a very high CIG penetration.

Keywords—Energy Storage System, Grid forming Control, Converter-Interfaced Generation, Damping, High Wind Penetration.

*Corresponding author, email: junru.chen.1@ucdconnect.ie

1 Introduction

1.1 Background

Electrical power systems are in the transition towards a 100% penetration of converter-interfaced generation (CIG), such as from solar panels and wind turbines. The replacement of traditional synchronous generators (SGs) by the CIGs reduces system inertia, thereby potentially leading to lower frequency support and potential frequency instability issues following a contingency or a sudden power imbalance in the grid [1]. In order to maintain the stability of the system under a high penetration of CIGs, it is desirable that at least some of the grid-tied converters have grid forming capability and provide either an emulated inertial response or a fast frequency regulation [2].

1.2 Literature review

The operation of CIG as grid forming converters implies the existence of an energy store which can be utilized to address supply-demand imbalance during transients, generally either in the form of an emulated inertia or droop response. Several possibilities exist for the provision of the energy store. De-loaded operation of the CIG is a method used to reserve a certain amount of the available power as “stored kinetic energy” by purposely setting the CIG operating point retarded or advanced from its optimum [3]. However, the disadvantage of this method is that it leads to an under-utilization of the renewable energy source. This has economic implications for the system and the CIG [4], since the renewable energy has the lowest marginal cost. Alternatively, virtual inertia control strategies in wind turbines can link the speed of the turbine to the grid frequency to extract the power from the energy stored in the rotating mass of the turbine. However, the kinetic energy released from the turbine reduces the rotor speed consequently resulting in generation reduction [5] and wind

energy waste for a long-term operation [6].

Alternatively in CIG, the transient power required during a disturbance can be supplied from the DC-link capacitance. In fact, the voltage variation on the DC-link capacitor of the grid-tied converter, has been shown to be equivalent to the inertial response of an SG [7] and a virtual inertia control has been proposed firstly in [8] and then improved in [9] and [10], which uses this DC voltage dynamic to emulate inertia. This approach, however, requires a large DC capacitor to provide sufficient inertia, thus making it more suitable for large high-voltage DC systems [11]. The combination of the renewable generation with an electrical energy storage system (ESS) provides the most flexible approach for establishing grid forming capability as its size can be chosen to provide adequate support and the support provided does not interfere with the optimum generation conditions. Under the assumption of sufficient DC side energy storage, grid forming controls, e.g. virtual synchronous generator (VSG) control [12], Virtual Synchronous Machine [13] or Synchronverter [14] have been applied to various different CIG systems. Relevant examples are PV plants [15], rooftop PV systems [16], wind turbines [17], wind farms [18], vehicle charger stations [19], hybrid PV-diesel systems [20] and DC Microgrids [21]. These can be integrated with ESSs [22] and supply droop freqeuncy control and inertia response [23]. Reference [24] comprehensively reviews the control strategies and implementations of the VSG.

In the case of wind turbines, the placement of an energy storage system, such as a battery storage on the DC side, requires modification to the wind turbine hardware and is therefore not an attractive solution for existing wind farms. Alternatively, the ESS can be placed on the AC side of the wind turbine (i.e. effectively just co-located with the turbine). In this case, the ESS alone can be controlled to be grid forming and provide the necessary frequency support during transients similar to the situation where the ESS is placed on the DC side. For example, reference [25] shows that similar capability for frequency support can be achieved by placing a VSG controlled ESS on the AC side of the wind turbine, while leaving the wind turbine configuration unchanged. Although

the grid forming and frequency support capability of this approach is similar to the DC side ESS, it has the major disadvantage that the variable renewable power generation does not go through the VSG control, so that it has no damping effect on the power fluctuations. This has an important effect on the overall system frequency variation in the case of systems with high penetration of variable renewable generation.

1.3 Motivation

In the literature, the ESS is generally assumed to be connected to the DC link of the generation system, with the generated power and the ESS power sharing the same VSG controlled converter interfacing to the grid. In this configuration, using VSG control, the ESS is in the middle (between the generation and grid) and can be considered as a filter to damp the stochastic power generation with the filtered power being stored in the ESS. However, the implementation of this approach in the existing CIG, which is typically operated in grid feeding mode, would require significant changes to the CIG system configuration which is costly and unnecessary. This work focusses on the implementation of the grid forming control on AC side ESS placement. Additionally, most of the previous work has focused on the support function of the grid forming CIG with DC side energy storage, after being subjected to a large disturbance. However, besides this transient response, the CIG should also mitigate the effect of the stochastic variation of the renewable generation on the frequency variance under normal operation. This is especially important in the situation where the power system is migrating to 100% CIG penetration [26]. Excessive frequency variation may cause unwanted tripping of the protection system which might ultimately result in a blackout. However, none of the previous works have investigated this aspect, nor has there been any work which shows how AC side ESS grid forming control can be co-ordinated with the wind turbine control to mitigate this effect. This paper addresses this gap.

1.4 Contribution

The main contribution of this work is to propose a novel VSG control approach that co-ordinates the renewable generator with the ESS placed at the AC side so as to properly emulate the inertial response of a synchronous machine and that also effectively damps power variations from the renewable generation. The effectiveness of this control scheme on reducing system frequency variation in a realistic, high renewable penetration system is investigated. The proposed control scheme also takes account of storage limitations and is shown to be effective for small ratios of the capacity of the ESS versus the capacity of the CIG. The effectiveness of the proposed approach is thoroughly demonstrated by means of simulation in a real power system, namely the all-Island Irish transmission system, which is a typical high-wind-penetration system.

1.5 Organization

The rest of paper is structured as follows: Section II reviews the VSG implementations and their coordination with the renewable generation. Section III introduces the proposed control method for the ESS at the AC side of the wind generation to damp the wind generation considering the rating of the ESS. Section IV verifies the proposed control via an EMT simulation based on Matlab/Simulink. Section V presents a system level simulation based on the Irish system and quantifies the benefits from the proposed control, while section VI draws the conclusions.

2 Virtual Synchronous Generator

The implementation of the VSG control for grid forming CIG has been extensively described in previous literature and here we only present a brief review necessary for the understanding of this work. The VSG control is an outer loop applied to the conventional voltage control of the voltage source converter which provides the reference for the voltage phase and magnitude. Under the assumption of operation in

a largely inductive gird, an active power regulation part determines the reference voltage phase, and a reactive power regulation part determines the reference voltage magnitude. A virtual impedance may also be included in the structure as shown in Figure 1.

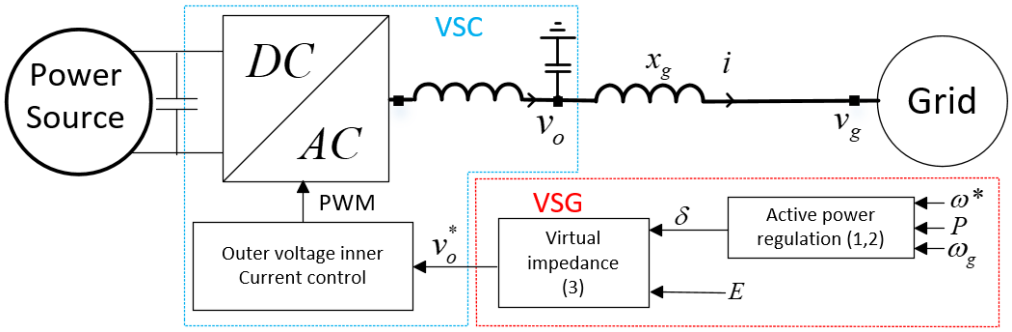

Fig. 1. VSG control scheme

In the active power regulation, the swing equation (1) is used for the converter synchronization and frequency to power droop (2) for the frequency support, where M is the virtual inertia, D is the damping factor, K_d is the droop gain, ω^* is the nominal frequency, ω_{pll} is the measured frequency from PLL and ω_{VSG} is the converter internal frequency. Note, the PLL here is only used for the droop control rather than the synchronization, and the measured frequency ω_{pll} follows the grid frequency quickly. During a transient state, the converter frequency ω_{VSG} is delayed in following the grid frequency change, thereby transiently leading to a larger phase difference δ between the converter voltage and grid voltage and, thus the output power, P, surges to provide an emulated inertia response. In steady state, the converter frequency is equal to the grid frequency and, thus, the power flow remains fixed at the reference. The reference power, P^*, is determined by the feed forward power from the renewable generation or is set to zero if there is no renewable generation and only an ESS connected.

$$\left.\begin{aligned} M\frac{d\Delta\omega_{VSG}}{dt} &= P^* + P_{droop} + D\Delta\omega_{VSG} - P \\ \dot{\delta} &= \Delta\omega_{VSG} \end{aligned}\right\} \quad (1)$$

$$P_{droop} = K_d(\omega^* - \omega_{pll}) \quad (2)$$

The reactive power regulation is used to determine the emulated electric potential E of the generator. Voltage to reactive power droop control or automatic voltage regulation can be applied.

The virtual impedance in the control loop can be considered to connect in series with the transmission line impedance and could be used to modify the R/X ratio, increase the system damping to aid stability or decouple the active and reactive power in a resistive line.

$$v_o^* = E\angle\delta - i(r_v + j\omega_{VSG}l_v) \quad (3)$$

The active power regulation determines the phase of the electric potential, and reactive power regulation determines the amplitude of the electric potential. After considering the voltage drop on the virtual impedance, the reference voltage for the conventional outer voltage, inner current control of the VSC can be obtained as (3). Here the details of the voltage control of the VSC are omitted as it follows a standard outer voltage, inner current control scheme implemented in the d-q frame as described in [27].

The active power P output from the VSG controlled converter consists of the reference power P^*, droop power P_{droop}, and transient inertia power ($D\Delta\omega_{VSG} - M\frac{d\Delta\omega_{VSG}}{dt}$), where the droop power and transient inertia power are provided by the ESS. The ESS can be placed either in the inner DC side (here referred to as VSGi) or the outer AC side (here referred to as VSGo) of the CIG system. Taking the full converter (type 4) wind turbine generator (WTG) as an example of the CIG system, the rest of this section will introduce the characteristics of these two configurations.

2.1 Inner energy storage system configuration

In the configuration of the VSGi as shown in Fig. 2, the ESS is placed on the DC side of the grid-tied converter (G-converter), where the VSG control is implemented. The machine-side converter (M-converter) operates with the maximum power point tracking (MPPT) control and is connected to the induction generator (IG), and the ESS-side converter (E-converter) is used to control the DC voltage. In this topology, the VSG control of the G-converter forms the voltage v_o supplying the power to the grid v_g. The reference power P^* in (1) is the renewable generation feed-forward power from the M-converter, so that the variable renewable generation is an input to the swing equation emulation and hence undergoes a damping effect. Thus, the whole VSGi system emulates the behaviour of a conventional SG in terms of power generation and frequency response. This configuration can damp the power supplied by the G-converter by means of a bi-directional exchange with the DC side ESS [28].

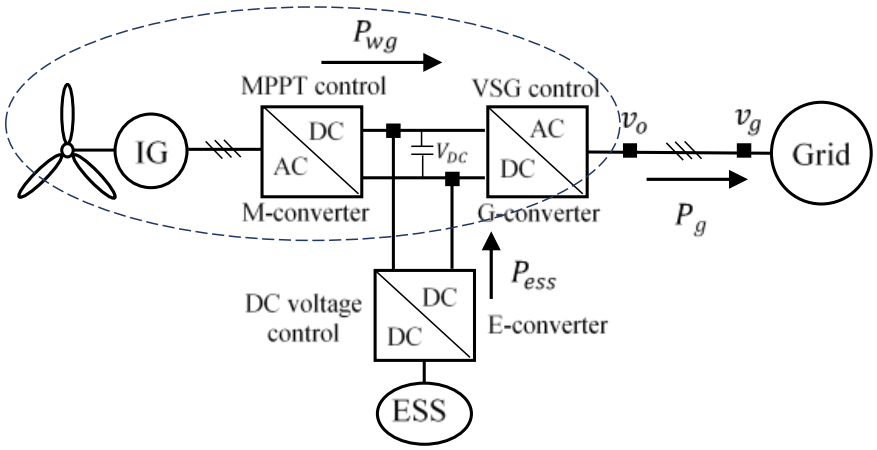

Fig. 2. VSGi system

2.2 Outer energy storage system configuration

In practice, most wind farms are already connected to the grid operating in grid feeding mode. For existing systems, the inclusion of the ESS at the DC side would require an increase in the G-converter capacity, which is costly and unfeasible. A compromise method is to place the ESS system externally at the AC side of the WTG system as shown in Fig. 3. In this topology, the original WTG system does not require

any change and remains operating in the current source mode feeding the generated power into the grid.

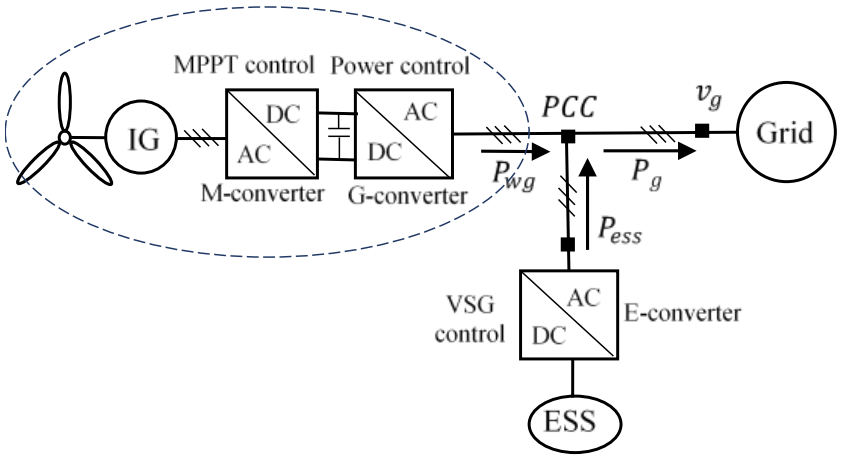

Fig. 3. VSGo system

The ESS system, although co-located with the WTG, can be regarded as a separate system and only used to support the frequency. Now with the VSG control applied only to the ESS, the measured power P in (1) is P_{ess}, reference power P^* is set to be zero, and only the droop power P_{droop} is an input and is damped by the swing equation of the VSG controlled E-converter. The grid power injection is simply a summation of the WTG generated power and ESS compensated power. Importantly, in this case the generated power is not input to the swing equation and is undamped. Hence, the dynamics resulting from the stochastic wind generation, act on the grid leading to an associated frequency variation.

The comparison between the VSGi and VSGo systems in terms their performance and their associated impacts on the system is presented via a Matlab/Simulink in Section IV and with a case study for the All-island Irish Transmission System in Section V.

3 Modified virtual synchronous generator control

The undamped power generation from the VSGo system contains significant oscillations due to the stochastic nature of the wind generation, which results in system frequency variation. The use of the VSGi configuration can alleviate this frequency variation due to the inclusion of the damping of the generation. In the VSGo system, since the ESS is closely linked to the WTG system, if the generated power goes into the ESS before being injected to the grid via the E-converter with VSG control, then this power can be damped. Of course, the power flow via the E-converter should be limited according to the capacity of the converter and storage. This section proposes a control to achieve such functions.

3.1 Modified VSGo system

Assuming the transmission line is a series inductive impedance X_g, and using the grid voltage V_g as a reference at zero rad, the power injected to the grid can be formulated as (4).

$$P = \frac{V_o V_g sin\alpha}{X_g} \tag{4}$$

Where $V_o\angle\alpha = E\angle\delta - i(r_v + j\omega_{VSG} l_v)$ represents the converter voltage previously mentioned in (3).

From (4), there are two equations with two parameters (grid voltage and line impedance), and four variables. If two of these variables are controlled, then the other two are automatically determined.

In the original WTG system, in grid feeding control, the power is directly controlled in the G-converter with its value being equal to the generated power. Thus, the converter voltage amplitude and phase are indirectly changed in order to deliver the required power. In this scheme, there is another loop needed to damp the power

generation from the WTG.

In the ESS system, under VSG control, the voltage amplitude and phase are directly controlled. The power flow is the consequence of the voltage difference between the converter and the grid. In this scheme, the phase is determined via the swing equation (1) with the dynamic response defined by the damping and inertia settings.

According to the above analysis, if we want to damp the wind power generation before injecting to the grid, the ESS has to determine the voltage at the point of common coupling (PCC) of the whole VSGo system in Fig. 3 and regulate the power flow between this point and the grid. On the other hand, in steady state, the power flow from the PCC to the grid should equal the WTG generation and ESS should not supply any power. To achieve this, the reference power in (1) can be changed to be the measured power being injected to the PCC from the WTG.

Fig. 3 can be used to illustrate the power generation in this configuration. Defining the generated power from the WTG is P_{wg}, the power from the ESS system is P_{ess}, and power injected into the grid is P_g. Initially assume that the grid is working at nominal frequency and no droop power is needed. At this time, the power being injected to the grid is the generated power and the ESS power is zero, while the reference power in (1) is the measured WTG power, i.e. (5).

$$P_{wg} = P^* = P_g = P_{wg0}; \quad P_{ess} = 0 \tag{5}$$

Subsequently, considering that the generated power from the WTG changes by ΔP, due to the damping and inertia (1), the phase from the PCC voltage to the grid cannot change instantly, thus the grid power injection remains the same. The change in generated power goes into and is stored by the ESS.

$$P_{wg} = P_{wg0} + \Delta P; \;\; P^* = P_g = P_{wg0}; \;\; P_{ess} = -\Delta P \tag{6}$$

After the VSG control detects the generation change and adjusts the reference

power, the phase changes smoothly as a consequence of the unbalanced power ($P^* \neq P_g$) in the swing equation and leads to the grid power injection changing to the generation value; this changed grid power injection comes from the ESS as indicated by (7). Here $G(t)$ is the transfer function from the reference power to the real power output, which is related to the virtual inertia, damping and impedance, detailed in [29]:

$$P_{wg} = P^* = P_{wg0} + \Delta P;\ \ P_g = P_{wg0} + \Delta P \cdot G(t);\ \ \ P_{ess} = -\Delta P + \Delta P \cdot G(t) \qquad (7)$$

When the output power flow equals the generated power, the ESS returns to a zero input, and the system stabilizes to a new steady operation point as presented in (8):

$$P_{wg} = P^* = P_g = P_{wg0} + \Delta P; \qquad P_{ess} = 0 \qquad (8)$$

In this process, the generated power is damped by the VSG controlled E-converter of the ESS. Since the swing equation becomes the same as that used in the VSGi operation, they would have the same response as viewed from the PCC point, even though their internal control structures are different

3.2 Excessive Power Regulation

In the proposed VSGo configuration, the change in power ΔP initially all goes into the ESS. Considering that in the worst case the maximum power change could be equal to the rating of the WTG, then the rating of the E-converter should be the same as the WTG in order to safely damp all the generated power. However, the principal function of the ESS is to provide frequency response, and for this function, the rating may not need to be so large. In this case, the maximum change in power cannot fully pass through the E-converter to be injected into the storage but can only partially do so. In this case, the system control should allow the maximum power which respects the E-converter rating to be injected into the storage, thus damping the generation as much as possible.

Defining P_m as the rating of the E-converter, if the changed power ΔP detected in (9) is greater than the ESS rating P_m, then the excess power P_{ex} (the difference between

the power change and the rating of the E-converter) should be injected into the grid directly and not passed via the ESS:

$$\Delta P = P_{wg} - P \tag{9}$$

$$P_{ex} = |\Delta P| - P_m \tag{10}$$

The PCC voltage is actively controlled and the power flowing into the grid is the consequence of the voltage difference in (4), where the converter voltage is determined by the VSG control in (1~3). In this case, in order to instantly deliver the excess power P_{ex}, the phase α has to change instantly. A PI controller (11) is used for this purpose as shown in Fig. 4, where K_p is used to link P_{ex} to α, and K_i is used to ensure the power is limited in the ESS as discussed in the next section.

$$G_{PI}(s) = K_p + \frac{K_i}{s} \tag{11}$$

3.3 PI Parameter Design

The VSG control can only directly regulate the phase δ of the electric potential, while the converter output voltage phase α is shifted by the virtual impedance. According to [29], the transfer function of the power change ΔP_g to voltage phase change $\Delta\delta$, considering the influence of the virtual impedance, can be expressed as:

$$H_L(s) = \frac{\Delta \mathrm{P}}{\Delta\delta} = \frac{3E_0}{2} \frac{a_1 s^2 + a_2 s + a_3}{(R^2 + X^2)[(R + sL)^2 + X^2]} \tag{12}$$

where $a_1 = U_{g0}LL_g(Rsin\delta_0 + Xcos\delta_0) - E_0LXL_g$; $a_2 = 2U_{g0}Lr_g(Rsin\delta_0 + Xcos\delta_0) - 2E_0LXr_g - U_{g0}L_v sin\delta_0(R^2 - X^2) + 2E_0L_vXsin\delta_0(Rsin\delta_0 - Xcos\delta_0)$; $a_3 = U_{g0}(R^2 + X^2)(Rsin\delta_0 + Xcos\delta_0) - 2U_{g0}R_vR^2 sin\delta_0 + 2E_0R_vXsin\delta_0(Rsin\delta_0 - Xcos\delta_0)$ and where E_0, V_{g0}, δ_0 are the initial equilibrium point values, and $R = R_v + R_g, X = X_v + X_g, L = L_v + L_g$. The poles of $H_{Line}(s)$ are at $-\frac{R}{L} \pm j\omega_g$, for which resonance occurs around the

grid synchronous frequency ω_g , where the phase changes from 0° to -180°.

The transfer function of the outer voltage inner current controls can be expressed as:

$$G_{VSC}(s) = \frac{\delta}{\delta_{ref}} = \frac{K_{pv}s + K_{iv}}{C_f t_i s^3 + C_f s^2 + K_{pv}s + K_{iv}} \tag{13}$$

Where t_i is the time constant of the closed-loop current controller, C_f is LC filter capacitance, K_{pv}/K_{iv} are the PI controller parameters of the voltage controller. The time constant of $G_{VSC}(s)$ is normally less than 10 ms, i.e. around 100 Hz, the phase of $G_{VSC}(s)$ change from 0° to -180° and the gain becomes negative from 0 dB.

The open-loop transfer function of the excess power regulation is:

$$G_{EX}(s) = (\frac{K_p s + K_i}{s}) G_{VSC}(s) H_L(s) \tag{14}$$

When the frequency approaches ω_g, the phase of $G_{EX}(s)$ turns to -180° and even lower due to $G_{VSC}(s)$ and $H_L(s)$. The PI controller of the excess power regulation has a corner frequency at $\frac{K_i}{K_p}$, where the phase turns from -90° to 0° and the slope turns from -20 dB/s to 0 dB/s. In order to ensure a satisfactory phase margin, the corner frequency of the PI controller should be less than ω_g. In this situation, at the lower frequency the system is mainly dominated by the PI controller, thus, $G_{VSC}(s)$ is negligible and $H_{Line}(s)$ acts as a pure gain:

$$H_{L,0} = \frac{3}{2} \frac{E_0 a_3}{(R^2 + X^2)^2} \tag{15}$$

The virtual impedance influences the value of $H_{L,0}$, the rationale for which has been detailed in [30]. The open-loop transfer function of the excess power regulation can be simplified to a second order system with crossover frequency:

$$G_{EX}(s) = \left(\frac{K_p s + K_i}{s}\right) H_{Line,0} \tag{16}$$

$$\omega_{\mathrm{co}} = \sqrt{\frac{K_i^2 H_L^2}{1 - K_p^2 H_L^2}} \tag{17}$$

In order to ensure the slope at crossover is greater than -20 dB/decade, ω_{co} should be less than the corner frequency $\frac{K_i}{K_p}$. Therefore, the condition for a stable operation of the excess power regulation can be summarized as:

$$\sqrt{\frac{K_i^2}{1 - K_p^2 H_L^2}} < \frac{K_i}{K_p} < \omega_g \tag{18}$$

Based on (16), the closed-loop transfer function of the excess power regulation is:

$$G_{EX,c}(s) = \frac{H_L K_p s + H_L K_i}{(H_L K_p + 1)s + H_L K_i} \tag{19}$$

The time constant of (19) is:

$$t_i = \frac{4(H_L K_p + 1)}{H_L K_i} \tag{20}$$

The time constant of the excessive power regulation should be as short as possible in order to quickly limit the ESS output.

When the power change is within the ESS limit, solely the VSG control is activated, as shown in Fig. 4, the transfer function G(s) of the VSG control used in (7) is:

$$G_{VSG}(s) = \left(\frac{1}{Ms + D} \cdot \frac{1}{s}\right) G_{VSC}(s) H_{Line}(s) \tag{21}$$

for which the stability was analysed in [19]. The VSG control scheme has to be modified to include the excess power regulation part, as shown in Fig. 4, where the blue part is the VSG control used to damp the unsaturated power generation, while the red part is the excess power regulation used to deliver the saturated power to the grid directly. This modified VSG control scheme is to replace the conventional VSG control scheme

in the active power regulation of Fig. 1 and control the converter phase angle δ.

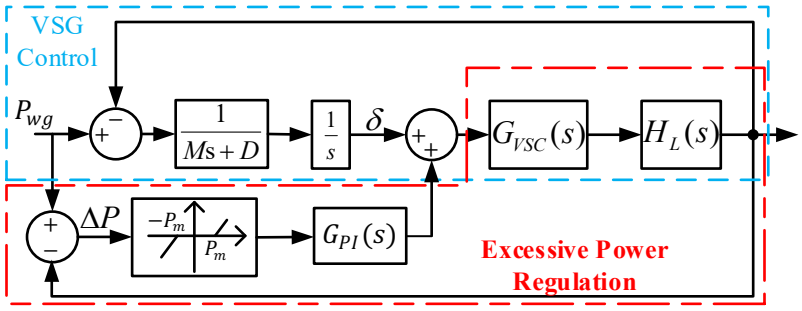

Fig. 4. Transfer function of the modified VSGo system.

4 EMT Simulation Validation

The proposed WTG configuration and its control are simulated in Matlab/Simulink using the EMT model of the converters. The WTG connects to the grid through a line impedance, where the wind turbine and battery in this simulation are assumed to be an ideal DC source and the grid is assumed to be an ideal AC source. The converter parameters and VSG parameters are given in Table I. There are two tests presented here. The first test compares the proposed WTG configuration with the other configurations, i.e., VSGo and VSGi, regardless of the rating of the ESS. The second test considers the rating of the ESS and verifies the operation of the proposed excessive power regulation.

TABLE I. VSG settings

Parameter	Value	Parameter	Value
Sampling time	1e-7 s	PWM rate	1350
Rated Voltage $\widehat{v_g}$	8165 V	Filter inductance	0.1 H
Reference voltage $\boldsymbol{V^*}$	8165 V	Filter resistance	0.12 Ω
Reference angular frequency $\boldsymbol{\omega^*}$	2π*50 Hz	Filter capacitance	13 μF
VSG Inertia **M**	2.6 kW/(rad·s^{-2})	Line inductance	0.1 H
damping/droop $\boldsymbol{K_d/D}$	159 kW/(rad·s^{-1})	Line resistance	0.01 Ω
Excess power controller P/I	3E-7 /5E-5	Virtual inductance	0 H
Current controller P/I	222/326	Virtual resistance	15 Ω
VSG and WTG PLL P/I	0.022/0.392	Voltage controller P/I	0.008/ 1.87

4.1 Test 1: wind turbine generator configurations

The aim of this test is to verify that the proposed control approach can make the outer ESS WTG combination have the same effect as the inner ESS WTG on both the power generation and frequency support. The VSGi and VSGo are used for comparison. To produce a fair comparison, the parameters are set identically for all configurations. The rating of the ESS is not limited in this test, thus, the power limit P_m in the proposed control (Fig. 4) is set to be infinite. The tested system experiences a wind power generation increase from 0 to 500 kW at 0.5 s and a grid frequency reduction from 50 Hz to 49.9 Hz with a 10 Hz/s ramp at 2 s. Fig. 5 shows the resulting grid power injection at the v_g in Fig. 2 and Fig. 3.

It can be seen from Fig. 5 that the power output in response to the grid frequency change is the same in all configurations (2~3.5 s), which indicates that similar frequency support can be provided regardless of the configuration of the WTG with ESS. This is as expected because the frequency variation presented to the swing equation (1) and droop (2) leads to power variation regardless of the ESS placement. However, the VSGi presents damping on the power generation, as its generated power goes through the swing equation (1), i.e. $P^* = P_w$. Without this action, i.e. $P^* = 0$, the generated power is injected into the grid instantly with a step change as presented in the VSGo case. In this context, the proposed method can make the VSGo behave like VSGi by forcing $P^* = P_w$ and resulting in the generated wind power flowing through the E-converter to the grid with the same damping. This verifies that the proposed method can add damping on the generation for the external ESS configuration, and the generated power flows accordingly (5~8) as expected.

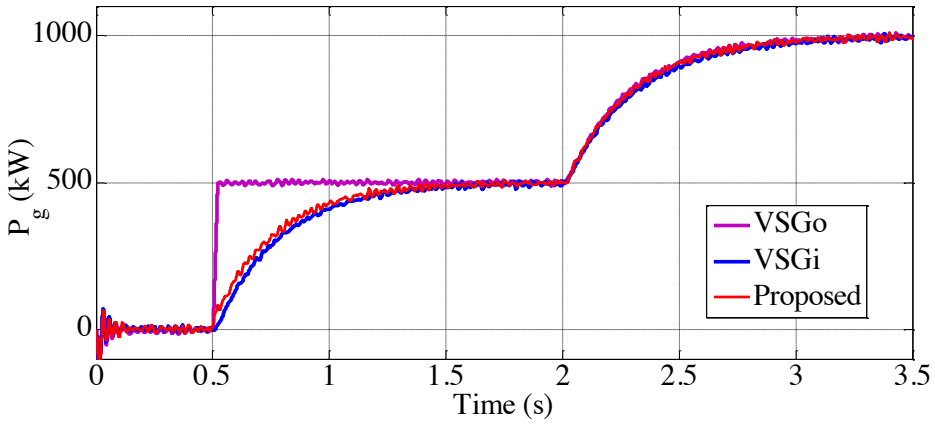

Fig. 5. Test 1: Grid power injection from different WTG configurations.

4.2 Test 2: Excess Power Regulation

This test aims to validate the excess power regulation function of the proposed method. In this test, the active power via the E-converter is limited at 200 kW, corresponding to P_m = 200 kW in Fig. 5. At 0.5 s, the generated power step increases to 500 kW from 0 kW. Fig. 6 shows the power from the E-converter P_{ess}, from the wind generator or G-converter P_{wg}, and to grid P_g.

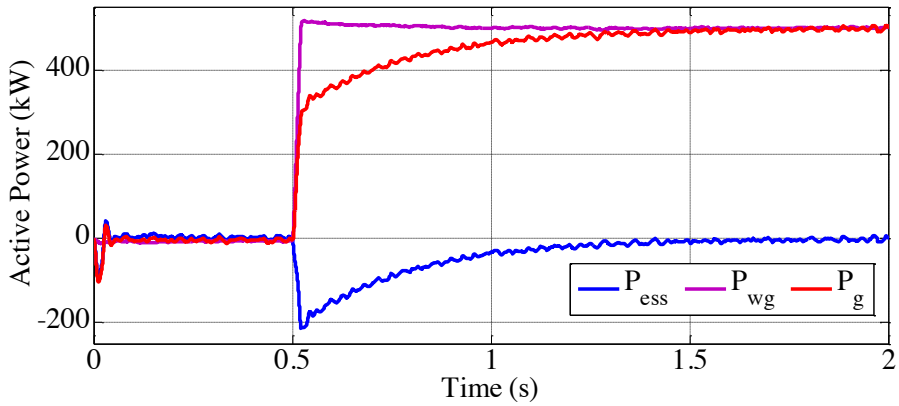

Fig. 6. Test 2: excess power regulation.

Figure 6 shows that the grid power injection P_g almost step changes (50 ms settling time as the designed reaction of the controller) to 300 kW at the instant of the generated power step change P_{wg} at 0.5 s, so that the power to the ESS P_{ess} is

suppressed within its limit. The rest of the power, 200 kW, still flows into the ESS at first and is damped by the E-converter of the ESS. This verifies the effectiveness of the proposed excess power regulation in respect with the rating limits for the operation of the ESS.

4.3 Test 3: Parameter Design

This test aims to verify the parameter design of the excessive power regulation. Based on the VSG settings listed in Table I, there are three cases with different PI parameters for the excessive power regulation as given in Table II, where:

- Case 1 is the base case which strictly fulfils the rules in Section 3.3 that the stability constrains are satisfied and the controller time constant is minimized.
- Case 2 is a comparative case which decreases K_i for a larger controller time constant but the stability constrains are still satisfied.
- Case 3 is another comparative case which breaks the stability constraints as the crossover frequency is greater than ω_g.

TABLE II. Excessive power regulation PI settings for Test 2

	K_p	K_i	ω_{co}(rad/s)	t_i(ms)
Case 1	3E-7	5E-5	206	55
Case 2	3E-7	5E-6	20.6	550
Case 3	3E-7	5E-4	2060	5.5

The system experiences the same changes as used in Test 2. Figure 7 shows the bode plot of the cases and Fig. 8 shows the results of the ESS output power in the time domain simulation. When the stability constraints are satisfied, the crossover frequency can be roughly predicted as shown in Fig. 7, and the system is stable as proved in Fig. 8. The crossover frequency is closer to ω_g, the stability margin is lowered.

However, since the time constant of the Case 2 is greater than that of the Case 1, Case 2 shows a higher peak power at the instant of the power change while Case 1 can better limit the ESS power output as shown in Fig. 8. On the other hand, when the stability constraints are not satisfied, i.e. $\omega_{co} > \omega_g$ as in Case 3, the phase sharply decreases below -180° at the synchronous frequency while the gain is still positive as shown in Fig. 7, thus the system is unstable as shown in Fig. 8. Note, in this case, the crossover frequency cannot be precisely predicted since the effect of the synchronous resonance is significant, and the transfer function analysis must use (14) but not (16).

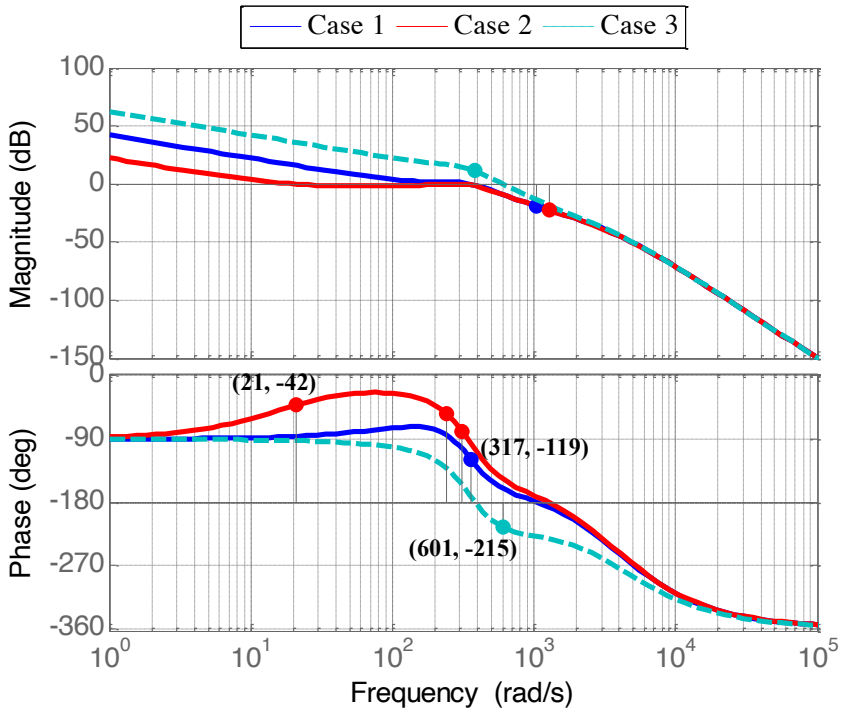

Fig. 7. Bode plot of these cases in Test 3.

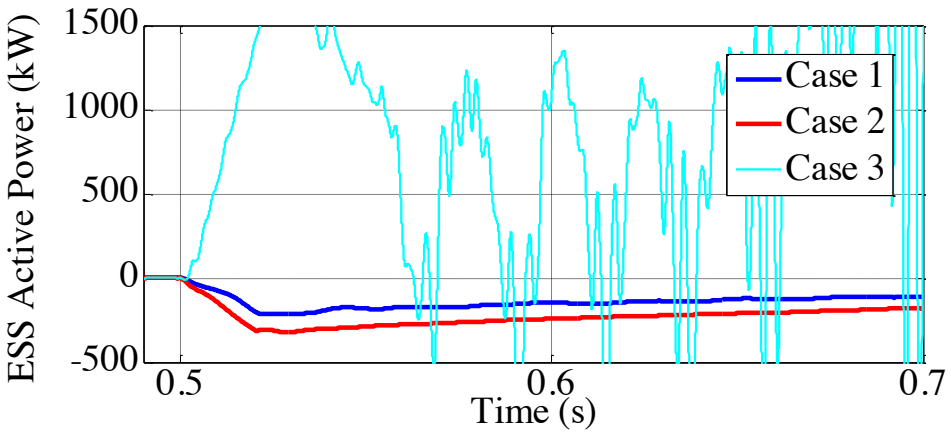

Fig. 8. Test 3: Parameter design.

5 Case Study

The Matlab/Simulink simulation in Section 4 is based on a two-bus system, which tests the CIG connected to an infinite bus, but this does not show the effect of the damped generation on the system frequency variations. In this section, we use the Irish transmission system as an example to demonstrate these effects, and furthermore to quantify the minimum total rating of the storage in the case of 100% wind penetration, in order to restrict the frequency variations within 50±0.2 Hz according to the Irish grid code requirement.

The model of the Irish transmission system consists of 1479 buses, 1851 transmission lines and transformers, and 245 loads. The dynamic models include 21 conventional synchronous power plants and 176 wind power plants. Reference [26] shows that the replacement of the SG in the system by VSG-controlled WTG with identical settings could achieve 100% wind penetration with the same stability level.

This paper focuses on the frequency variations resulting from the VSG controlled WTG and storage combination in a 100% non-synchronous generation case, thus, all of the SGs are replaced by the WTGs combined with ESS as given in [26]. Note, in the case study, the VSG uses AVR for the voltage stability. The overall system loading is 2.36 GW. The wind input is set to be stochastic using the Weibull distribution model for all the WTGs and the load is also set to be stochastic using the Ornastein-

Uhlenbeck's process [31] with ±5% of variation to their original values.

A Monte Carlo analysis is used where 100 simulations are run for each case in DOME, a Python-based power system software [32]. The grid frequency is measured by the centre of inertia (COI). Two cases are presented in the paper, the first one verifies the effectiveness of the proposed outer ESS WTG operation strategy, compared with the VSGo and VSGi results; the second one analyses the effect of the ESS rating on the frequency variations and, particularly, quantifies the minimum rating of the ESS required to damp the generation at this loading.

5.1 Case 1: wind turbine generator configurations

In this case, the paper compares the frequency variations from the stochastic wind and loads in the Irish system under different WTG configurations, i.e., VSGo, VSGi and the proposed method. The rating of the ESS is not limited in this case. Fig. 9 shows that the use of VSGo in the Irish system leads to a significant frequency variance of ±0.26 Hz, while the application of the VSGi can reduce this variance by 50% to ±0.13 Hz. Fig. 9(c) verifies the effectiveness of the proposed control to reduce frequency fluctuations compared to the conventional VSGo scheme. The dynamic behaviour of the proposed control is comparable with that of the conventional VSGi scheme. It is noticed that for the Irish system, the normal system frequency variance should be within ±0.2 Hz. Clearly, the use of the VSGo with conventional control does not satisfy this but the VGSo with the proposed control does.

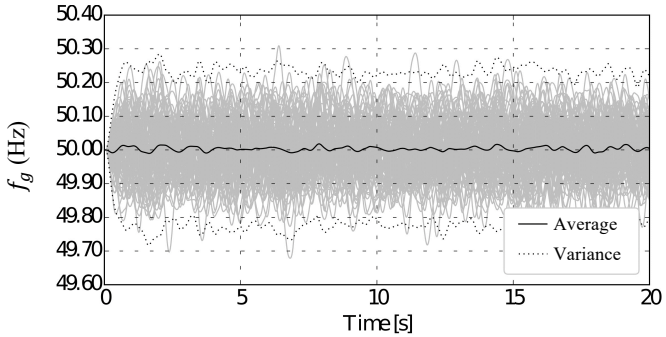

(a) VSGo result – grid frequency

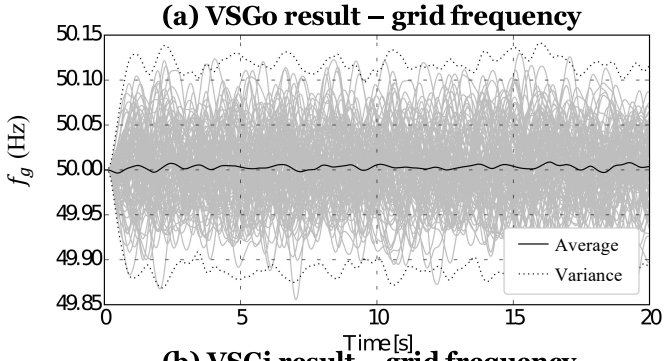

(b) VSGi result – grid frequency

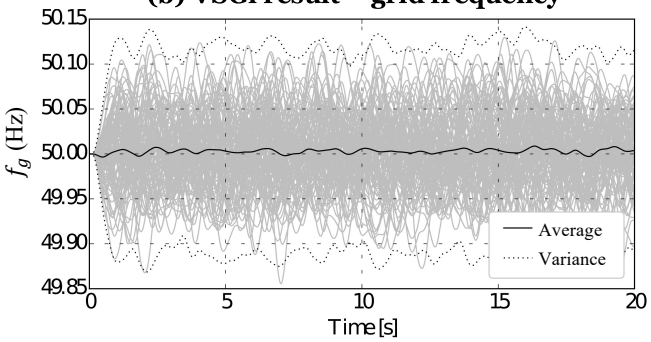

(c) Proposed WTG configuration – grid frequency

Fig. 9. Case 1 result: WTG configurations effects on the frequency variations.

In order to illustrate the origin of the different frequency variance in these configurations, Fig. 10 presents the grid power injection from one of the WTG systems in one of the scenarios. It can be seen that, compared with the VSGo, the power injection from the VSGi is smoother. The proposed method achieves the same power response as the VSGi. The variation of power injected to the grid results in the frequency variance. This is the reason that the VSGo shows higher system frequency variance than the VSGi and the proposed method.

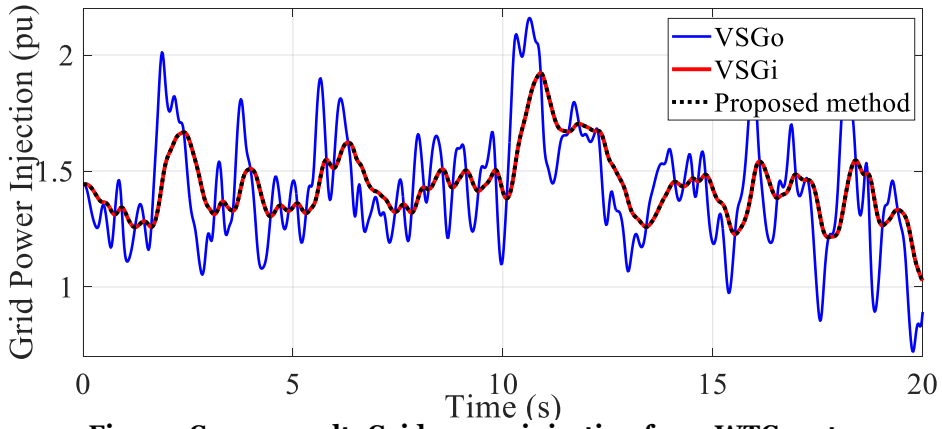

Fig. 10. Case 1 result: Grid power injection from WTG systems.

5.2 Case 2: limited energy storage system rating

In the previous results, the proposed VSG control has been shown to damp the wind generation from the co-located ESS, and limit the ESS power flow to avoid overload of the ESS. This case aims to investigate the effect of the ESS rating on the frequency variance. To investigate this the rating of the ESS is gradually reduced from 100% of the WTG initial power to 0% and the results of the frequency variance are recorded in Fig. 11.

Figure 11 shows that the increase of the ESS rating from 0% provides a considerable improvement in the frequency variance initially, but this improvement becomes saturated with further increase in the ESS rating with no further improvement is achieved beyond an ESS rating greater approximately 20%. In other words, as long as the ESS rating is greater than 21% of the WTG power generation, then it is possible to damp all of the generated power. This is because only the change in generated power flows through the ESS, rather than the initial power which is delivered to the grid directly.

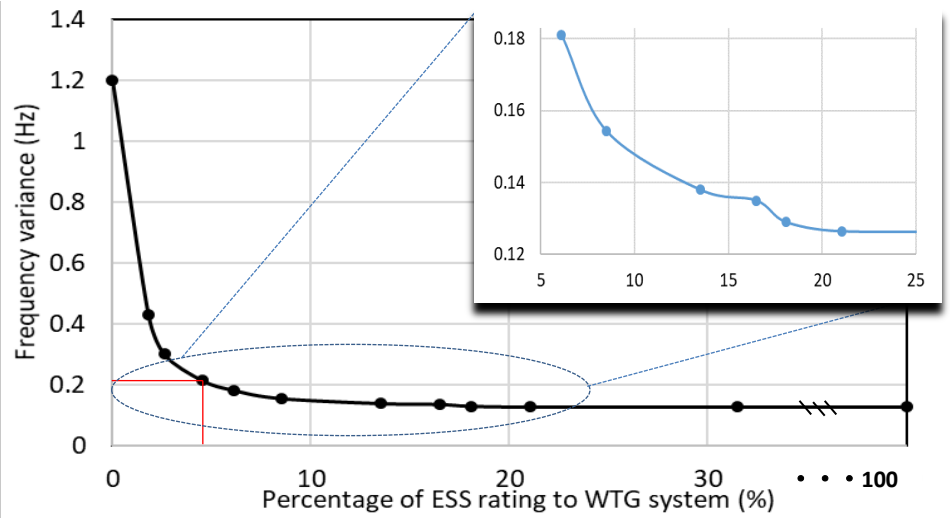

Fig. 11. Case 2 result: ESS rating vs. frequency variance.

To meet the requirement of the grid code on the ±0.2 Hz frequency variance, the rating of the ESS should be at least 5% of the WTG initial power. On the other hand, it should be noticed that the frequency variance in the no ESS situation (1.21 Hz) is higher than that in the VSGo situation presented in case 1 (0.26 Hz). This is because, in the case of the VGSo, although the generated power is not damped, the resulting frequency variance is still reacted to by the ESS and this helps alleviate this variance. However, due to the inertia and damping, the VSG time constant (2 s) is greater than the frequency of the wind oscillation (0.5 s), so that the ability of this frequency support is limited. Most of the frequency variance reduction should still rely on the damping of the generation directly, which is achieved by the proposed method.

Figure 12 presents the grid power injection of one of the WTG systems in one of the scenarios for various different ESS ratings of 4.7%, 13.4% and 100%. The increase in the ESS rating smooths the grid power injection. Notably, the 13.4% ESS rating scenario has a very similar performance to the power generation with the 100% scenario.

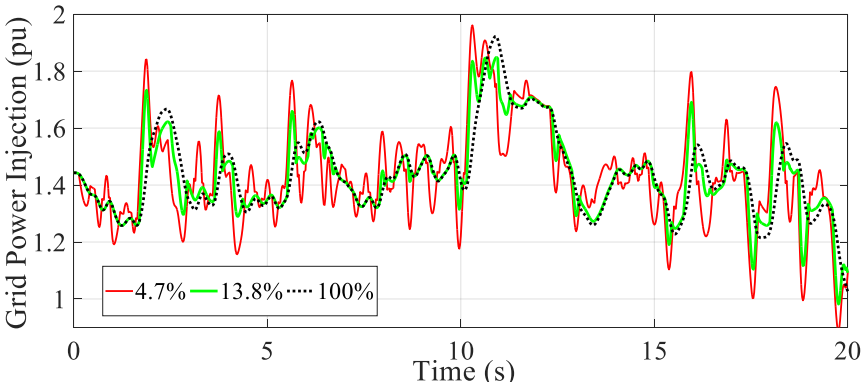

Fig. 12. Case 2 result: Grid power injection from WTG systems.

In order to further explain such a phenomenon that a small quantity of the ESS can adequately damp the wind generation dynamics, the probability density of the wind generation at one of the WTG systems in all the 100 scenarios has been plotted in Fig. 11, where the x-axis is the generated power variation expressed as a percentage of its mean value and the y-axis is the probability of occurrence of each of the variations. This wind power variation is computed from the power deviation from its average using the case with no ESS. Nearly 90% of the wind generation variation occurs within a ±20% band of the mean value, thus a corresponding value of the ESS rating (22.6% in Fig. 11) can almost damp all of the generation. The highest probability of the wind power variation is around ±5%, which is the reason for the curve of Fig. 9 to exhibit a sharp change in the frequency variance level when the ESS comprises around 5% of the WTG initial power.

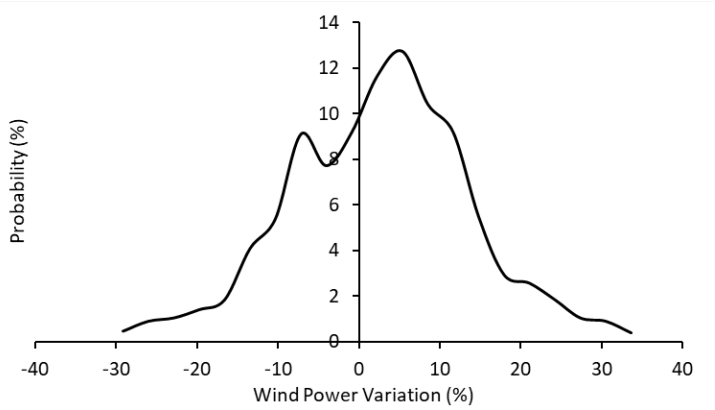

Fig. 13. Probability of the wind power variation in percentage.

6 Conclusions

This paper proposes a modified virtual-synchronous-generator control method for the outer energy storage system co-located with wind generators. The proposed coordinated control effectively damps the power fluctuations of the wind turbines and properly takes into account the limited capacity of the energy storage system. Importantly, the proposed control method only involves the energy storage system and does not require any modification in the controllers of the wind power plant. Yet, it achieves the same performance as the system where the storage is connected internally to the DC side of the converters of the wind turbines. The case study of the all-island Irish transmission system serves to prove that the proposed method can effectively mitigate the frequency variations caused by the stochastic renewable generation and only a relatively small capacity of the energy storage system is required to make the proposed control effective. The results would indicate that the storage capacity needs to be about the size of the variance of the stochastic fluctuations of the power generated by the wind power plants, e.g., in Irish system, if the power rating of the ESS is over 5% of the WTG initial power, the grid code requirements relating to frequency variance can be satisfied.

Acknowledgements

This work is partly funded by the Science Foundation Ireland (SFI) under grant numbers SFI/15/SPP/E3125 and SFI/15/IA/3074, and by the European Commission, under the project EdgeFLEx, grant no. 883710.

.

References

[1] J. Đaković, M. Krpan, P. Ilak, T. Baškarad, and I. Kuzle, “Impact of wind capacity share, allocation of inertia and grid configuration on transient RoCoF: The case of the Croatian power system,” *International Journal of Electrical Power & Energy Systems*, Vol. 121, Oct. 2020, pp.1-8.

[2] F. Milano, F. Dörfler, G. Hug, D. J. Hill and G. Verbič, "Foundations and Challenges of Low-Inertia Systems (Invited Paper)," *2018 Power Systems Computation Conference (PSCC)*, Dublin, Ireland, 11-15 June, 2018, pp. 1-25.

[3] J. Liu, Z. Yang, J. Yu, J. Huang, and W. Li, “Coordinated control parameter setting of DFIG wind farms with virtual inertia control,” *International Journal of Electrical Power & Energy Systems*, vol. 122, pp. 1-11, November 2020.

[4] H. Wang, Z. Chen, and Q. Jiang, “Optimal control method for wind farm to support temporary primary frequency control with minimised wind energy cost,” *IET Renewable. Power Generation*, vol. 9, no. 4, pp. 350–359, May 2015.
[5] Y. Wang, J. Meng, X. Zhang and L. Xu, "Control of PMSG-Based Wind Turbines for System Inertial Response and Power Oscillation Damping," *IEEE Transactions on Sustainable Energy*, vol. 6, no. 2, pp. 565-574, April 2015.
[6] D. Ochoa and S. Martinez, "Fast-Frequency Response Provided by DFIG-Wind Turbines and its Impact on the Grid," *IEEE Transactions on Power Systems*, vol. 32, no. 5, pp. 4002-4011, Sept. 2017.
[7] I. Cvetkovic, D. Boroyevich, R. Burgos, Chi Li, M. Jaksic and P. Mattavelli, "Modeling of a virtual synchronous machine-based grid-interface converter for renewable energy systems integration," *2014 IEEE 15th Workshop on Control and Modeling for Power Electronics* (COMPEL), Santander, Spain, 22-25 June, 2014, pp. 1-7.
[8] L. Huang, H. Xin, Z. Wang, K. Wu, H. Wang, J. Hu, et al., "A Virtual Synchronous Control for Voltage-Source Converters Utilizing Dynamics of DC-Link Capacitor to Realize Self-Synchronization," *IEEE Journal of Emerging and Selected Topics in Power Electronics*, vol. 5, no. 4, pp. 1565-1577, Dec. 2017.
[9] J. Fang, H. Li, Y. Tang and F. Blaabjerg, "Distributed Power System Virtual Inertia Implemented by Grid-Connected Power Converters," *IEEE Transactions on Power Electronics*, vol. 33, no. 10, pp. 8488-8499, Oct. 2018.
[10] J. Fang, H. Li, Y. Tang and F. Blaabjerg, "Distributed Power System Virtual Inertia Implemented by Grid-Connected Power Converters," *IEEE Transactions on Power Electronics*, vol. 33, no. 10, pp. 8488-8499, Oct. 2018.
[11] Y. Cao, W. Wang, Y. Li, Y. Tan, C. Chen, L. He, et al., "A Virtual Synchronous Generator Control Strategy for VSC-MTDC Systems," *IEEE Transactions on Energy Conversion*, vol. 33, no. 2, pp. 750-761, June 2018.
[12] T. Shintai, Y. Miura and T. Ise, "Oscillation Damping of a Distributed Generator Using a Virtual Synchronous Generator," *IEEE Transactions on Power Delivery*, vol. 29, no. 2, pp. 668-676, April 2014.
[13] S. D’Arco, J. A. Suul, and O. B. Fosso, “A Virtual Synchronous Machine implementation for distributed control of power converters in SmartGrids,” *Electric Power Systems Research*, vol. 122, pp. 180-197, May 2015.
[14] Q. Zhong and G. Weiss, "Synchronverters: Inverters That Mimic Synchronous Generators," *IEEE Transactions on Industrial Electronics*, vol. 58, no. 4, pp. 1259-1267, April 2011.
[15] W. Ming and Q. Zhong, "Synchronverter-based transformerless PV inverters," *IECON 2014 - 40th Annual Conference of the IEEE Industrial Electronics Society*, Dallas, TX, 29 Oct.-1 Nov., 2014, pp. 4396-4401.
[16] S. Mishra, D. Pullaguram, S. A. Buragappu, and D. Ramasubramanian, “Single-phase synchronverter for a gridconnected roof top photovoltaic system,” *IET Renewable Power Generation*, vol. 10, no. 8, pp. 1187-1194, May 2016
[17] Q. Zhong, "Virtual Synchronous Machines: A unified interface for grid integration," *IEEE Power Electronics Magazine*, vol. 3, no. 4, pp. 18-27, Dec. 2016.
[18] Q. C. Zhong, Z. Ma, W. L. Ming, and G. C. Konstantopoulos, “Grid-friendly wind power systems based on the synchronverter technology,” *Energy Conversion and Management*, vol. 89, pp.719-726, January 2015.
[19] J. A. Suul, S. D'Arco and G. Guidi, "Virtual Synchronous Machine-Based Control of a Single-Phase Bi-Directional Battery Charger for Providing Vehicle-to-Grid Services," *IEEE Transactions on Industry Applications*, vol. 52, no. 4, pp. 3234-3244, July-Aug. 2016.
[20] A. Belila, Y. Amirat, M. Benbouzid, E. M. Berkouk, and G. Yao, “Virtual synchronous generators for voltage synchronization of a hybrid PV-diesel power system,” *International Journal of Electrical Power & Energy Systems*, vol.117, pp.1-14, May 2020.
[21] D. Chen, Y. Xu and A. Q. Huang, "Integration of DC Microgrids as Virtual Synchronous Machines Into the AC Grid," *IEEE Transactions on Industrial Electronics*, vol. 64, no. 9, pp. 7455-7466, Sept. 2017.

[22] J. Chen, M. Liu and T. O'Donnell, "Replacement of Synchronous Generator by Virtual Synchronous Generator in the Conventional Power System," *2019 IEEE Power & Energy Society General Meeting* (PESGM), Atlanta, GA, USA, 4-8 Aug., 2019, pp. 1-5.
[23] K. M. Cheema, A. H. Milyani, A. M. EI-Sherbeeny, and M. A. EI-Meligy, "Modification in active power-frequency loop of virtual synchronous generator to improve the transient stability," *International Journal of Electrical Power & Energy Systems*, vol. 128, pp. 1-9, June 2021.
[24] K. M. Cheema, "A comprehensive review of virtual synchronous generator," *International Journal of Electrical Power and Energy Systems*, vol. 120, pp.1-10, September 2020.
[25] J. Chen, M. Liu, F. Milano and T. O'Donnell, "Placement of Virtual Synchronous Generator Controlled Electric Storage combined with Renewable Generation," *2019 IEEE Milan PowerTech*, Milan, Italy, 23-27 June 2019, pp. 1-6.
[26] J. Chen, M. Liu, F. Milano, and T. O'Donnell, "100% Converter-Interfaced generation using virtual synchronous generator control: A case study based on the irish system," *Electric Power Systems Research*, vol. 187, pp. 1-10, Octorber 2020.
[27] A. Yazdani and R. Iravani, "Voltage-Sourced Converters in Power Systems: Modeling, Control, and Applications", John Wiley & Sons, Canada, ISBN 978-0-470-52156-4, 2010.
[28] Y. Yang, J. Xu, C. Li, T. Dragicevic, and F. Blaabjerg, "Stability enhancement of DC power systems by VSM control strategy," *International Journal of Electrical Power & Energy Systems*, vol. 126, p. 106569, 2021.
[29] J. Chen and T. O'Donnell, "Parameter Constraints for Virtual Synchronous Generator Considering Stability," *IEEE Transactions on Power Systems*, vol. 34, no. 3, pp. 2479-2481, May 2019.
[30] J. Chen and T. O'Donnell, "Analysis of virtual synchronous generator control and its response based on transfer functions," *IET Power Electronics*, vol. 12, no. 11, pp. 2965–2977, 2019.
[31] F. Milano and R. Zárate-Miñano, "A Systematic Method to Model Power Systems as Stochastic Differential Algebraic Equations," *IEEE Transactions on Power Systems*, vol. 28, no. 4, pp. 4537-4544, Nov. 2013.
[32] F. Milano, "A python-based software tool for power system analysis," *2013 IEEE Power & Energy Society General Meeting*, Vancouver, BC, 21-25 July, 2013, pp. 1-5.